Supporting Information

Hexagonal Prism Arrays Constructed by Ultrathin Porous Nanoflakes of Carbon Doped Mixed-Valance Co-Mn-Fe Phosphides for Ultrahigh Areal Capacitance and Remarkable Cycling Stability

Richao Niu,[a,b] Gengjie Wang,[b] Yuying Ding,[b] Shaochun Tang,[b,*] Xiangkang Meng,[b] Xuemin Hu,[a] Junwu Zhu,[a,*]

[a] Key Laboratory for Soft Chemistry and Functional Materials, Ministry of Education, Nanjing University of Science and Technology, Nanjing 210094, P. R. China

[b] National Laboratory of Solid State Microstructures, Collaborative Innovation Center of Advanced Microstructures, College of Engineering and Applied Sciences, Department of Materials Science & Engineering, Nanjing University, Jiangsu, 210093, P. R. China

*Correspondence and requests for materials should be addressed to S.C. Tang (tangsc@nju.edu.cn), or J.W. Zhu (zhujw@njust.edu.cn).

Experimental Section

Pretreatment of Ni Foam: Ni foam was cut with size 3 × 1 cm^2 and immersed in 1 M HCl solution to remove the surface NiO by sonication for 10 min. Ni foam was subjected to sonication in deionized water to remove the excess of HCl. And it was rinsed with acetone, ethyl alcohol, and deionized water. Finally, the treated Ni foam was then freeze dried.

Carbon-Doped Hierarchically Hexagram Precursors: All chemical reagents were analytical grade and used without further purification. Typically, 2 mmol of cobaltous sulfate hexahydrate ($CoSO_4•7H_2O$), 0.5 mmol of iron sulfate hexahydrate ($FeSO_4•7H_2O$), 0.5 mmol of manganese sulfate hexahydrate ($MnSO_4•H_2O$), 6 mmol of hexamine ($C_6H_{12}N_4$), 2 mmol of ammonium fluoride (NH_4F), and 0.01 M glucose were dissolved in 40 mL of distilled water under continuous stir until the color from pink to orange-yellow. This resulting in a mixed solution contain Co^{2+}, Fe^{2+}, and Mn^{2+} being 50 mM, 12.5 mM, and 12.5 mM, respectively. Then the mixed solution and a cleaned Ni foam were transferred to 50 mL Teflon-lined stainless steel autoclave, and maintained at a constant temperature of 120℃ for 8 h. After the autoclave was cooled naturally, the precursor-covered Ni foam was wished in an ultrasound bath and finally freeze dried.

Carbon-Doped Hierarchically Hexagram Porous C-doped CFMP Arrays: In the subsequent phosphating process, the obtained precursors (C-doped CFMOOH on Ni foam) were put into a furnace with sodium hypophosphite at 350 ℃ for 2 h. Through anion-exchange, hexagram-like porous C-doped Co-Mn-Fe phosphides (C-doped CFMP) hexagram arrays were obtained. For comparison, Co-Mn-Fe phosphides (CFMP) and Co-Mn phosphides (CMP) were also prepared via the above-mentioned process under the same conditions as those for C-doped CFMP.

Nitrogen doped graphene (NG) hydrogel: Graphene oxide (GO) was obtained by a modified Hummer's method. A homogeneous dispersion with a GO concentration of 4 mg mL^{-1} was obtained by dispersing dry GO power at an ultrasound power of 100

W in deionized water for 2 h. Under continuous stir, 1 mL ethylenediamine was added over 15 min, as the reductant and the N-dopant source. Then 30 mL of the mixture was transferred to a 50 mL Teflon-lined autoclave and kept at 180 °C for 12 h. The resulting cylindrical NG hydrogel was cleaned by immersion in DI water for 12 h.

Materials Characterizations: The morphologies of the as-synthesized products were observed by field-emission scanning electron microscopy (FE-SEM, Hitachi S-4800). Microstructure information was analyzed via transmission electron microscopy (TEM) on a transmission electron microscope (TECNAI F20) at 200 kV acceleration voltages. Crystal structure of the C-doped CFMOOH and C-doped CFMP was obtained by X-ray diffraction (XRD) with radiation of Cu target (Kα, β = 0.145 nm). The surface elemental species and valence of the prepared samples were characterized by X-ray photoelectron spectroscopy (XPS) of Thermo Fisher Scientific with Al Kα X-ray source (1486.6 eV).

Electrochemical Measurements: The electrochemical behaviors were tested in 1 M KOH aqueous electrolytes. In the three-electrode measurements, the Ni foam supported C-doped CFMOOH and C-doped CFMP (10 mm×10 mm) was directly served as working electrode, a platinum and Ag/AgCl were acted as counter and reference electrodes. Cyclic voltammetry (CV), galvanostatic charge-discharge (GCD), and electrochemical impedance spectroscopy (EIS) tests were carried out on an electrochemical workstation (VMP3 workstation Biologic France). Cycle life was evaluated on a LAND CT2001A test system by GCD techniques. The CV and GCD curves of single electrode were recorded with the potential range of -0.2 to 0.6 V.

Specific capacitance (C_s) of the electrode materials was calculated by the equation: $C_s = I \cdot \Delta t / (\Delta V \cdot S)$, where I is the discharge current (A), Δt is the discharge time (s), ΔV is the potential range of GCD (V), and S is the effective area of the electrode (cm^{-2}). Coulombic efficiency is calculated as $\eta = t_d / t_c \times 100\%$, where t_c and t_d are the charge and discharge times, respectively. The loading mass of active materials in the electrodes is 0.35, 0.35, 0.36 mg cm^{-2} for C-doped CFMP, CFMP, and CMP, respectively.

Asymmetric Supercapacitor (ASC): The Ni foam supported CFMP arrays acted as the positive electrode and Ni foam supported NG film as negative electrode separated by the filter paper with soaked by 1 M KOH solution. As for the negative electrode, the NG hydrogel was cut into rectangular strips and pressed on a nickel foam under a pressure of 6~8 MPa to form a film. For asymmetric devices, it is essential to balance the charges of the two electrodes. The mass ratio was determined according to the charge balance equation ($q^+ = q^-$). To obtain this, the masses of the positive and negative electrodes were balanced according to the equation: $m^+ / m^- = C_g^- \Delta V^- / C_g^+ \Delta V^+$, where m is the mass, C_g is the specific capacitance, and ΔV is the voltage range for positive and negative electrodes. The mass ratio of m (C-doped CFMP) / m (NG) was about 0.2. The ASC device was packaged in button battery case. The energy and power density were calculated as follows: $E = 1 / 2CV^2$, $P = E / t$, where E is the energy density; P is the power density; C is specific capacitance of ASCs.

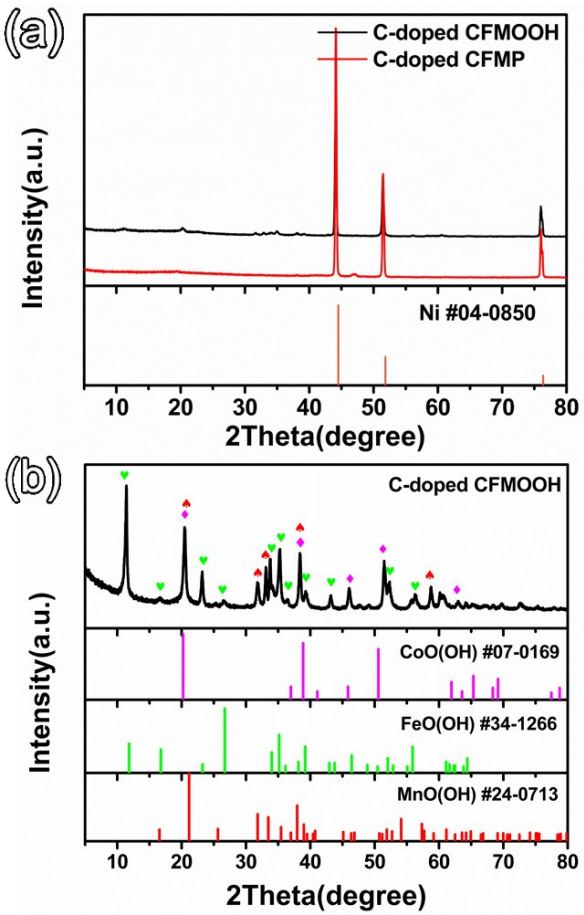

Figure S1. XRD patterns of (a) C-doped CFMOOH, C-doped CFMP on a nickel foam and (b) C-doped CFMOOH.

The patterns of C-doped CFMOH and C-doped CFMP on nickel foam are showed in Figure S1a. Although the intensity according to nickel is high, the characteristic diffraction peaks for C-doped CFMOOH is still observable. In order to obtain the phase of the sample, the sample was scraped from the nickel foam surface for testing. XRD patterns obtained from the C-doped CFMOOH products are presented in Figure S1b. The diffraction peaks should be assigned to the hexagonal structure of CoO(OH) (JCPDS No. 07-0169), orthorhombic structure of MnO(OH) (JCPDS No. 24-0713), and tetragonal structure of FeO(OH) (JCPDS No. 34-1266). Among these phase, it was found that there is a difference in the peak strength of FeO(OH). Generally, the

peak strength indicates the crystallinity of different crystal face, and the temperatures, doping elements and orientation growth have a great influence on it.[1-4] Hence, with the combined influence of F^- ions and $C_6H_{12}N_4$, the unique hexagonal structure formed because of the directional growth of grains.

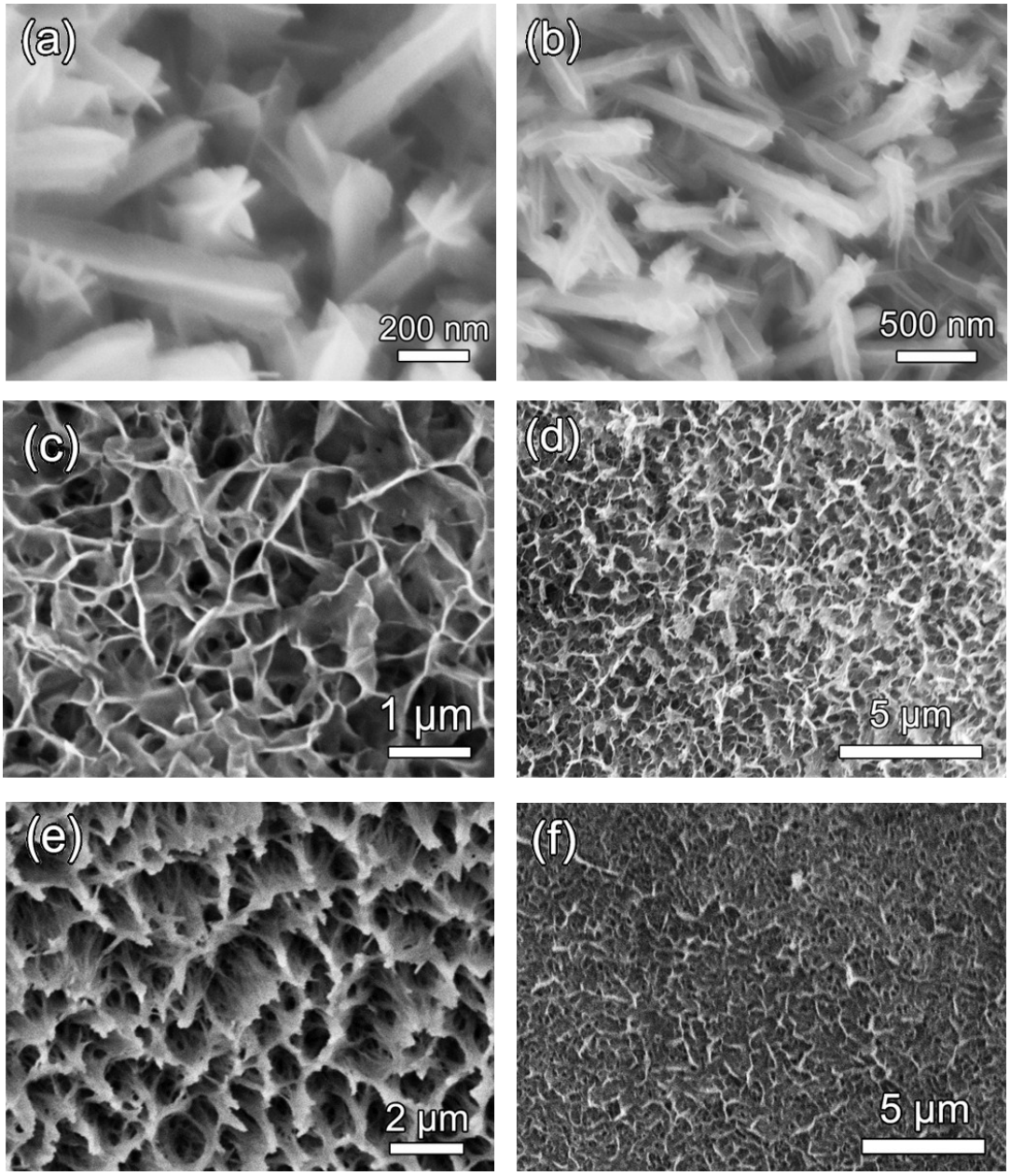

Figure S2. SEM images of (a) CFMOOH, (b) CFMP and (c, d) CFMOOH HPAs obtained with mixed solvent of glycol and water (1:1), (e, f) SEM images of precursor without NH_4F and HMTA, respectively, while other parameters were remained.

As shown in Fig. S2e and f, the nanorod arrays formed without NH_4F would agglomerate with each other and no hierarchical hexagonal structure can be observed. Meanwhile, in the absence of $C_6H_{12}N_4$, irregular nanoflakes are formed instead of the hexagonal prism arrays on nickel foam. Hence, the combined roles of F^- ions and $C_6H_{12}N_4$ result in the formation of hierarchical hexagonal structure.

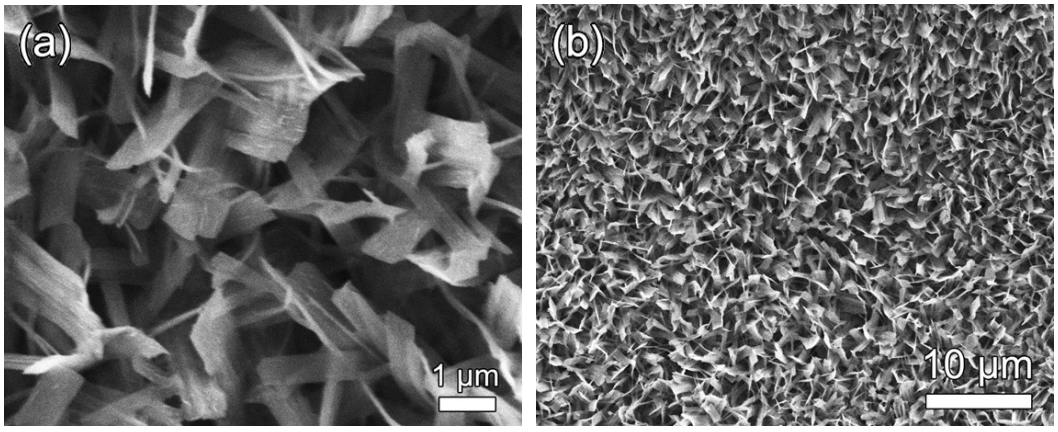

Figure S3. SEM images at different magnifications of CMOOH arrays on a Ni foam.

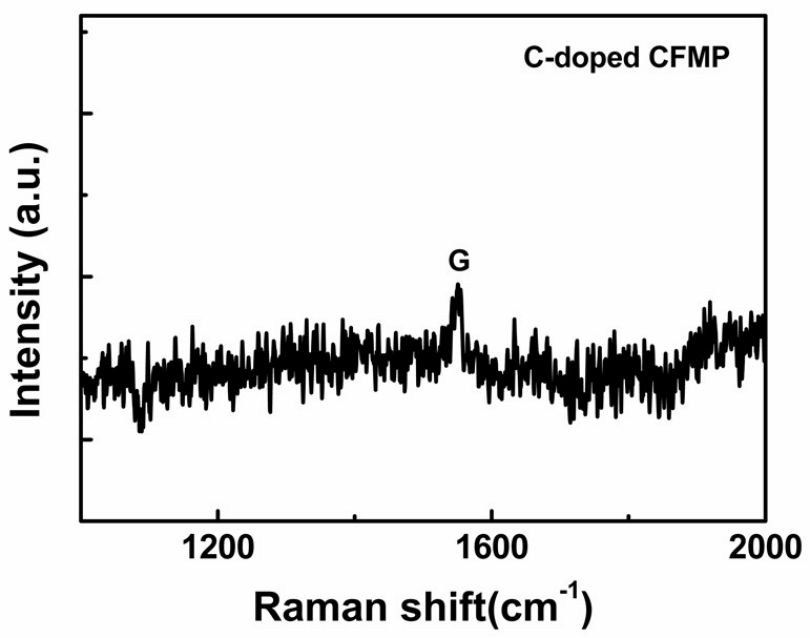

Figure S4. Raman spectrum of C-doped CFMP.

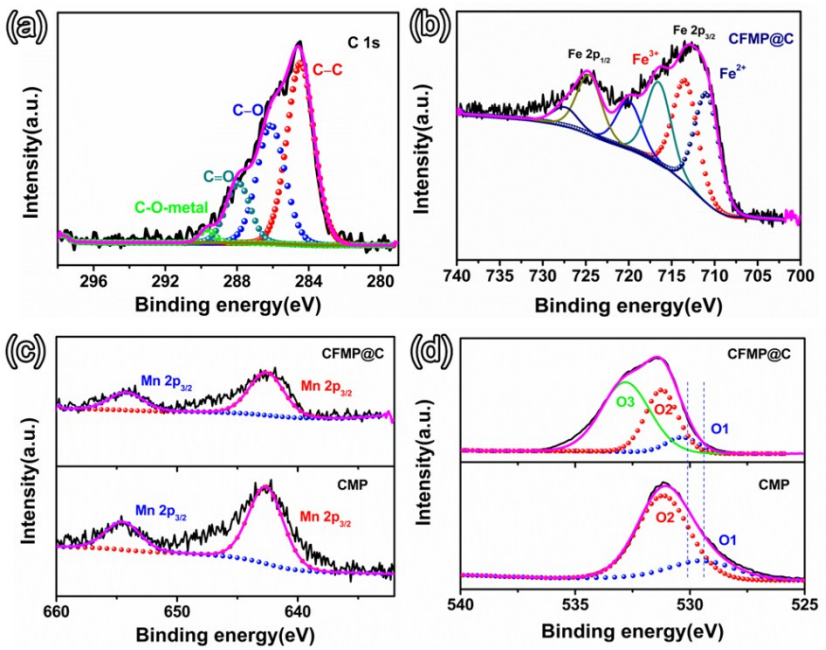

Figure S5. High resolution XPS spectra (a) C 1s, (b) Fe 2p, (c) Mn 2p, and (d) O 1s, which were recorded from the typical C-doped CFMP.

.

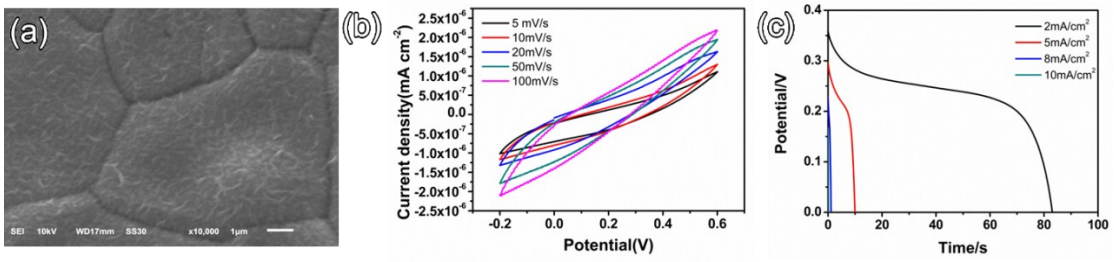

Figure S6. (a) A SEM image of bare nickel foam after a hydrothermal process without any metal salt while other parameters were remained. (b) Cyclic voltammetry curves, and (c) galvanostatic charge-discharge curves of bare nickel foam.

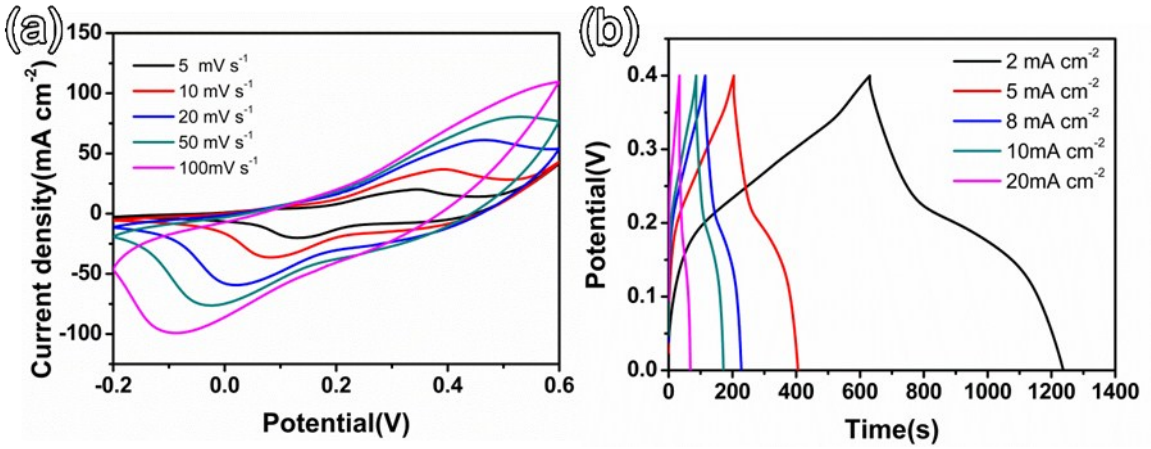

Figure S7. (a) CV curves and (b) GCD curves of CMP without Fe element while other parameters were remained.

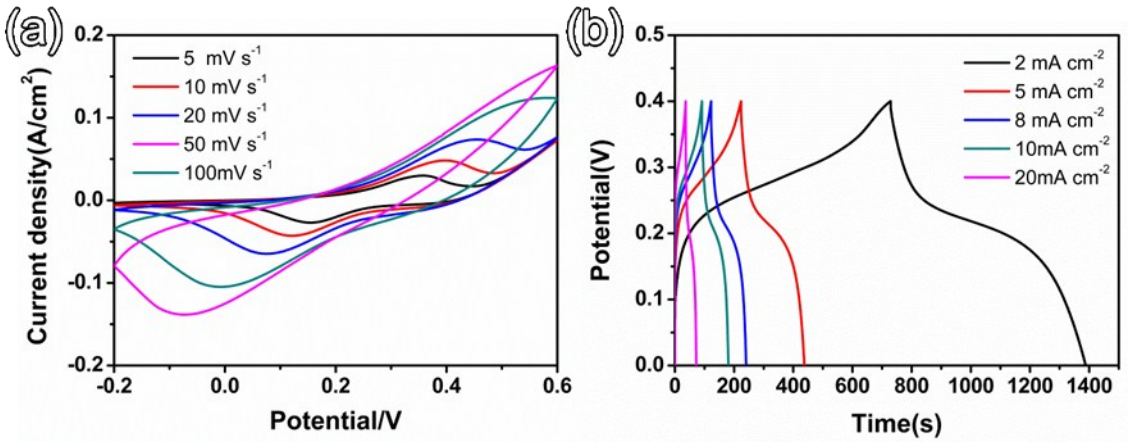

Figure S8. (a) CV curves and (b) GCD curve of CFMP without carbon doping.

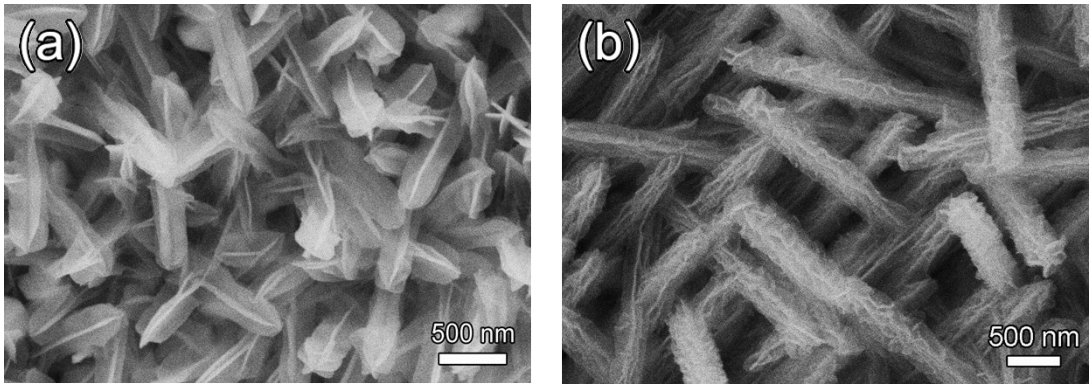

Figure S9. SEM images of (a) C-doped CFMP and (b) CFMP HPAs after 5000 discharge/charge processes

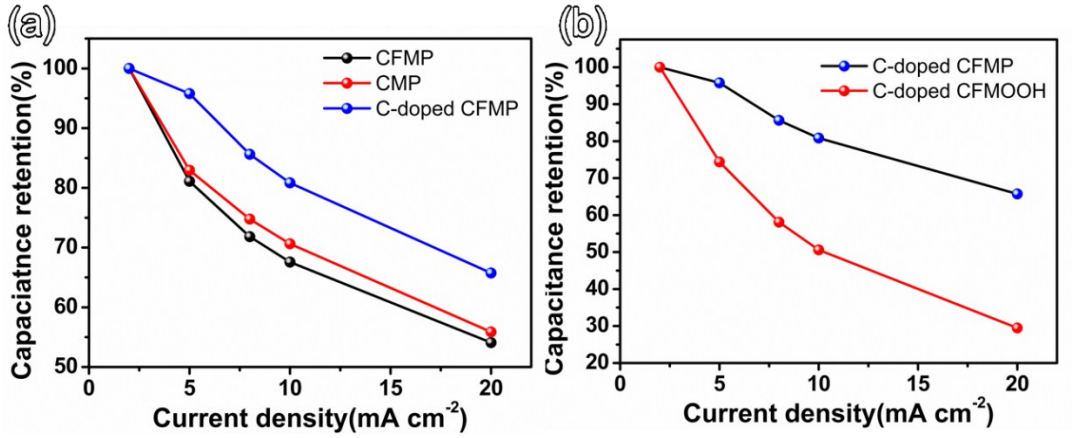

Figure S10. (a, b) Specific capacitance values of C-doped CFMP, CFMP, CMP and C-doped CFMOOH electrodes versus specific current densities from charge–discharge curves.

As shown in Fig. 10a, the C-doped CFMP electrode has higher capacitance retention rate compared with the CFMP and CMP electrodes when the current increases from 2 to 20 mA cm^{-2}. Notably, the C-doped CFMP electrode after phosphating exhibits more excellent conductivity and higher specific capacitance rate retention about 65% than precursor (30%) with increasing current densities (Fig. S10b). This result indicates that the more porous and rough nanoflakes formed after phosphating facilitate the transfer of electrolyte ions and permeation with active materials, even during rapid charging and discharging processes.

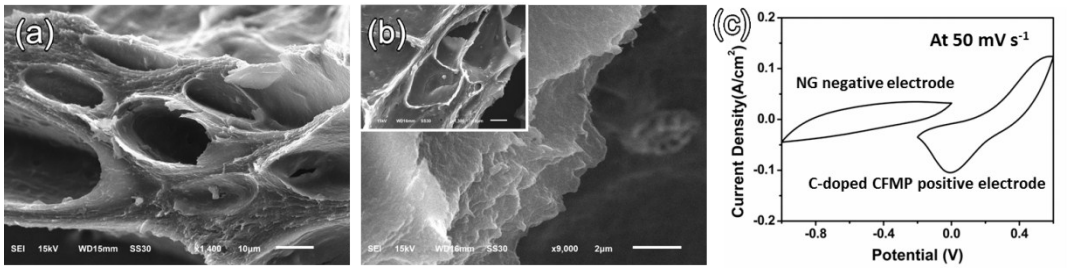

Figure S11. (a, b) SEM images of NG with different magnifications. (c) CV comparison of C-doped CFMP and NG electrodes with different potential windows measured at a scan rate of 50 mV s^{-1}.

References

1. L. F. Chen, Z. Y. Yu, J. J. Wang, Q. X. Li, Z. Q. Tan, Y. W. Zhu and S. H. Yu, *Nano Energy*, 2015, **11**, 119–128.
2. Z. Y. Zhang, C. G. Bao, W. J. Yao, S. Q. Ma, L. L. Zhang and S. Z. Hou, *Superlattices Microstruct.*, 2011, **49**, 644–653.
3. X. M. Sun, X. Chen, Z. X. Deng and Y. D. Li, *Mater. Chem. Phys.*, 2002, **78**, 99–104.
4. S. Y. Kuo, W. C. Chen, F. Lai, C. P. Cheng, H. C. Kuo, S. C. Wang and W. F. Hsieh, *J. Cryst. Growth*, 2006, **287**, 78–84.